VI International Conference on Particle-based Methods – Fundamentals and Applications
PARTICLES 2019
E. Oñate, M. Bischoff, D.R.J. Owen, P. Wriggers & T. Zohdi (Eds)

EXPERIMENTAL AND NUMERICAL INVESTIGATIONS ON PARAMETERS INFLUENCING ENERGY DISSIPATION IN PARTICLE DAMPERS

Niklas Meyer[1], **Robert Seifried**[1]

[1] Institute of Mechanics and Ocean Engineering, Hamburg University of Technology
Eißendorfer Straße 42, 21073 Hamburg, Germany
n.meyer@tuhh.de/robert.seifried@tuhh.de, www.tuhh.de/mum

Key words: Particle damping, Complex power, Energy dissipation, DEM

Abstract. Particle damping has become a favorable passive damping technique for lightweight structures, however, its complex dimensioning process hinder its wide use in technical applications. An experimental based model and a numerical model are developed in order to investigate the energy dissipation of the dampers regardless of the underlying structure. The experimental model consists only of the particle box with a free-free boundary condition, which is excited by a harmonic force. Via the complex power, the loss factor and the energy dissipation are obtained. A corresponding numerical discrete element model is developed. With these models, a large frequency and acceleration range is analyzed. Different filling ratios of the particle box are investigated, indicating the high potential of particle dampers for different excitation ranges. First comparisons of experiments and simulations showing a good qualitative agreement, enabling the simulation as a future design tool for particle dampers.

1 Introduction

One favorable passive tool to reduce vibrations of technical applications is the utilization of particle dampers being a derivative of impact dampers. Instead of using only one impact object, dozens or even thousands of particles might be included in a single particle damper. Thus, the particle size normally ranges from the micrometer scale to the millimeter scale. Either a box or a hole in the vibrating structure serves as a particle container. The structural vibrations are transferred via the container walls onto the particles. Interactions between particles and between particles and the container walls cause an energy dissipation by impacts and frictional phenomena, resulting in vibration attenuation.
Particle dampers show several advantages when compared to other existing passive damping techniques [1]. However, despite the efficiency of particle dampers, they have been used only in a few different engineering applications so far mostly designed for a very specific system. This might be due to the fact, that the physical processes in the particle dampers are complex and highly nonlinear. These processes are not fully understood yet

and depend on a variety of different influence parameters, like the excitation frequency, the vibration amplitude, the filling ratio of the container and the used materials. These dependencies make the optimal design of particle dampers so far very burdensome and time intensive due to empiric parameter tuning.
Particle dampers might be analyzed utilizing a specific underlying vibrating structure [2]. Instead, in this paper investigations are performed concerning the energy dissipation of particle dampers directly, by excluding the underlying structure. The obtained experimental and numerical results and insights provide a tool for a target-oriented particle damper design. Therefor, an experimental based model and a numerical model for the particle damper are introduced. Both models consist only of the particle box with a free-free boundary condition, which is excited by a harmonic force. The complex power is calculated by the velocity signal and the excitation signal. Via the complex power, the loss factor and the energy dissipation are obtained. A large frequency range (40 Hz - 1 kHz) and acceleration range (10 $\mathrm{m/s^2}$ - 400 $\mathrm{m/s^2}$) is investigated.
For the numerical model the discrete element method is used. The simulations help to identify the interdependent parameters affecting the energy dissipation of particle dampers. Particles are considered as unconstrained moving bodies only influenced by their interactions. The experiments are compared with the numerical results. The influence of the different contact parameters are analyzed. A good qualitative agreement is achieved by using a velocity dependent coefficient of restitution and sliding friction.

2 Experimental model

In [2] particle dampers are analyzed utilizing an underlying vibrating structure. Here, the energy dissipation of particle damper alone is investigated, i.e. without an underlying structure. Thus, a corresponding testbed is developed, see also [3]. A systematic representation and a picture of these are shown in Fig. 1. The concept of the testbed is a particle box with a free-free boundary condition and excited by a controlled harmonic force via a shaker. The excitation force is controlled such, that the frequency and acceleration magnitude of the box stays constant. Via the measured velocity of the box and the measured force of the shaker, the complex power is determined [4]. By the complex

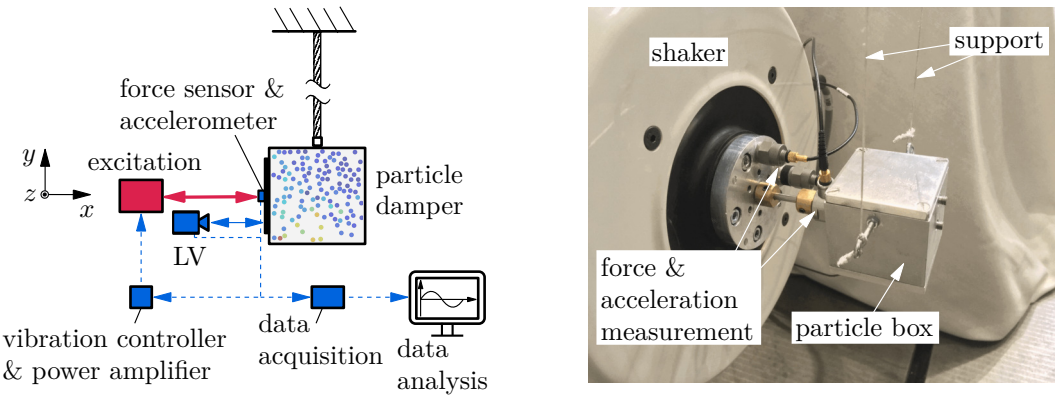

Figure 1: Systematic representation (left) and picture (right) of the testbed.

power, the energy dissipation and the loss factor can be calculated.
The box is made of aluminum with a cubical shape and an inner edge length of 4 cm. The free-free boundary condition is accomplished by two ropes. The force sensor, the accelerometer, and the control system are from BRÜEL & KJAER. While the box is excited by the LDS V455 shaker, its acceleration is controlled via the LDS Comet system. Due to the impacting particles on the box walls, the acceleration signal is very noisy. In order to use this acceleration signal in the control of the excitation, the accelerometer is additionally equipped with a mechanical low-pass filter. It consists of a plastic tube with a Young's modulus of $86\,\mathrm{N/mm^2}$. This filter element is designed in a way that its eigenfrequency ω is at 2.5 kHz. Hence, the single particle impacts on the box walls are filtered efficiently, as their contact frequency is normally significantly above 5 kHz. Simultaneously, frequencies up to the measurement range of 1 kHz are only little influenced.
The velocity of the particle box is measured via a laser vibrometer (LV), the PSV-500, from POLYTEC. The data acquisition of the velocity and force signals are accomplished by the Front-End of the PSV-500 with a sampling frequency of 250 kHz. The second accelerometer, seen in Fig. 1 (right), is not equipped with a filter as it is only used for triggering the measurement. The feasible measurement range of the system is between 40 Hz till 1 kHz and between $10\,\mathrm{m/s^2}$ till $400\,\mathrm{m/s^2}$. The measurement range is divided into a logarithmic grid of 108 points. Nine frequencies and twelve acceleration values are used and each combination is measured for 2.5 s.

3 Complex power

For the determination of the dissipated energy and the loss factor, the complex power P, introduced for particle damper analysis by Yang [4], is used and briefly summarized here. Given a harmonic excitation, the complex power follows to

$$P = \frac{1}{2} F V^* . \tag{1}$$

Hereby, F denotes the fast Fourier transform (FFT) of the force signal and V^* the conjugate FFT of the velocity signal. The dissipated power P_{diss} and the maximum power stored in a cycle P_{max} follow from the complex power as

$$P_{\mathrm{diss}} = \mathrm{Real}(P) = \frac{1}{2}|F||V|\cos(\phi_{\mathrm{F}} - \phi_{\mathrm{V}}), \tag{2}$$

$$P_{\mathrm{max}} = \mathrm{Imag}(P) = \frac{1}{2}|F||V|\sin(\phi_{\mathrm{F}} - \phi_{\mathrm{V}}). \tag{3}$$

The phase angles of the force and velocity signals are denoted by ϕ_{F} and ϕ_{V} respectively. To obtain the dissipated energy per radiant E_{diss} the dissipated power is divided by the excitation frequency Ω as

$$E_{\mathrm{diss}} = \frac{P_{\mathrm{diss}}}{\Omega}. \tag{4}$$

The loss factor η is defined as the ratio of the dissipated power to the maximum power stored in a cycle as

$$\eta = \frac{P_{\mathrm{diss}}}{P_{\mathrm{max}}} = \frac{\mathrm{Real}(P)}{\mathrm{Imag}(P)}. \tag{5}$$

4 Discrete Element Method

The Discrete Element Method (DEM) is a discrete simulation method for granular materials. The DEM has been developed by Cundall and Strack [5] for the simulation of systems consisting of discs and spheres. Its general concept can be used for any system of many unconstrained particles where the system behavior is governed by the contacts between these particles [6]. While in general the particles can have an arbitrary shape, for efficiency purpose mostly spherical particles are used in the simulations. Every particle is considered as an unconstrained moving body only influenced by applied forces. The dynamics are obtained by setting up Newton's and Euler's equation of motion for every particle [7]. For spherical particles, this reads

$$m_i \ddot{\boldsymbol{x}}_i = \boldsymbol{F}_i, \quad \boldsymbol{I}_i \dot{\boldsymbol{\omega}}_i = \boldsymbol{M}_i \quad (i = 1, ..., N), \tag{6}$$

with $\ddot{\boldsymbol{x}}_i$ and $\dot{\boldsymbol{\omega}}_i$ being the translational and rotational accelerations. The particle mass is denoted by m_i and its diagonal inertia tensor by $\boldsymbol{I}_i$, whereby all three entries of $\boldsymbol{I}_i$ are identical. The applied forces and moments are denoted by $\boldsymbol{F}_i$ and $\boldsymbol{M}_i$, and N is the total number of particles. The Eq. (6) is in general a coupled nonlinear differential equation with $6N$ degrees of freedom for 3D simulations. Particle systems often contain a large number of particles (up to thousands or millions). During the time integration, all existing contacts need to be detected and resolved in every time step. Therefore, efficient detection algorithms and contact laws are needed. Also, the choice of an appropriate time integration scheme is crucial [6]. In this research, the algorithms presented in [2] are used and only shortly introduced.

4.1 Contact forces

In DEM simulations, particle-particle and particle-wall continuous contacts occur. The contact partners are treated as rigid, thus only touching in a single point. In continuous contact modeling, the contact partners i and j are allowed to overlap, and virtually connected by unilateral springs and dampers, as shown in Fig. 2. Hereby, the corresponding contact forces occur which counteract the overlap δ_{ij}. For the calculation of the contact forces, various models have been developed [8, 9, 10]. The contact law of Hertz [8] is widely used for a sphere-sphere contact, as it is based on physical parameters, namely the Young's modulus $E_{i/j}$ and the Poisson's ratio $\nu_{i/j}$. Later on, the result of Hertz was extended by a dissipative term [9, 10]. In the simulations, the formula of Gonthier [10] for the normal contact force is used, which reads,

$$F_{\mathrm{N},ij} = k_{ij} \delta_{ij}^{3/2} \left(1 + \frac{\bar{d}}{e} \frac{\dot{\delta}}{\dot{\delta}_{\mathrm{a}}} \right). \tag{7}$$

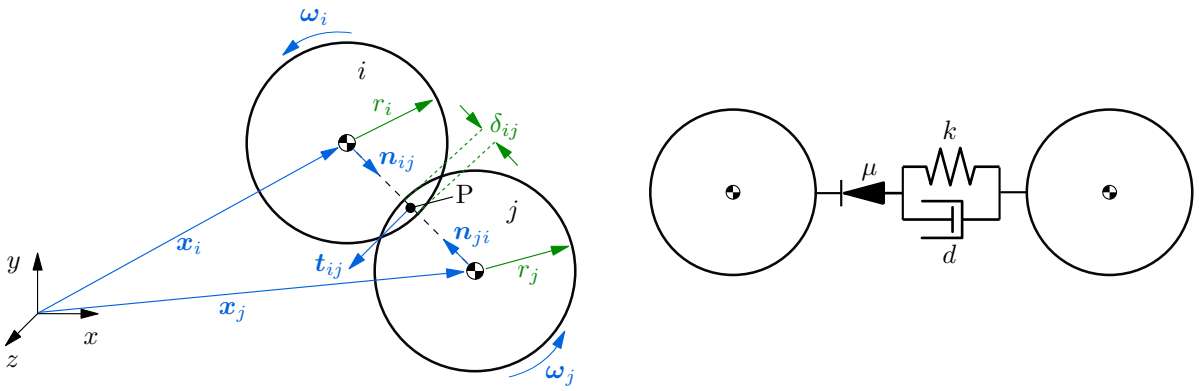

Figure 2: Contact states (left) and contact model (right) of two spheres.

Hereby, the contact stiffness and the material parameters are given as

$$k_{ij} = \frac{4}{3\pi(h_i + h_j)} \sqrt{\frac{r_i r_j}{r_i + r_j}}, \tag{8}$$

$$h_{i/j} = \frac{1 - \nu_{i/j}^2}{\pi E_{i/j}}. \tag{9}$$

The penetration velocity and the initial penetration velocity in normal direction are denoted as $\dot{\delta}$ and $\dot{\delta}_\mathrm{a}$ respectively. The coefficient of restitution e ($0 < e < 1$) controls the amount of energy dissipation during the contact. In contrast to other contact models, e.g. Lankarani [9], the formula of Gonthier (7) can be applied to nearly the complete range of e. The nonlinear parameter $\bar{d}$ is only depending on e and can be solved once offline [10]. For spherical particles, the tangential forces result only from sticking and sliding friction, whereas the resistance of the surface is described by the coefficient of friction μ. For highly dynamical systems the sticking friction can be neglected [6]. When only sliding friction is considered, a smoothing hyperbolic tangent function can be used, in order to avoid jumps in the friction forces at zero velocity, see [11]. The sliding friction reads

$$\boldsymbol{F}_{\mathrm{R},ij} = -\mu |F_{\mathrm{N},ij}| \boldsymbol{t}_{ij} \tanh(\tau |\boldsymbol{v}_{\mathrm{P},ij}^{\mathrm{t}}|), \tag{10}$$

with $\boldsymbol{v}_{\mathrm{P},ij}^{\mathrm{t}}$ being the relative, tangential velocity at the boundary point P and τ as the smoothing parameter. The tangential direction is denoted by $\boldsymbol{t}_{ij}$. The resulting torques on the particles are only depending on the friction forces, as the normal forces are always pointing towards the center of mass of the particles. For comparison also sticking friction is implemented, see [12]. However, in the simulation this model is much more time consuming.

4.2 Contact detection and time integration

Another very important component of the DEM is the contact detection. All existing contacts have to be determined in every time step. A variety of algorithms have been developed for this task, such as sort-based, cell-based, or tree-based ones, decreasing the

complexity to an optimum of $\mathcal{O}(N)$. In the program, the verlet list in combination with the link cell algorithm is used [7].
Also, the time integrator has a big influence on the simulation speed and the overall stability. As the contact detection and evaluation of the contact forces are most time-consuming in DEM simulations, the numerical effort for the time integrator itself is often negligible. But, its choice has a big influence on the number of evaluations of the equation of motion. In this research, good results with the fifth order Gear predictor-corrector algorithm [13] have been achieved.

4.3 Coefficient of restitution calculation using FEM

In DEM simulations often a constant coefficient of restitution (COR) is used. Indeed, this is in reality not the case, as the COR depends on a variety of influence parameters. These influence parameters are mainly associated with the energy dissipation effect. For the used metals (S235 and Al6060) in this work, the energy dissipation comes mainly from plastic deformations in the contact zone. Thus, the impact velocity has a big influence on the COR. There exist different investigations on the COR, as for instance in [14, 15, 16]. In this work, the FEM-approach and material data from [16] are used. Metals often behave elastic-viscoplastic. This means, that the plastic flow also depends on the strain-rate. For the material description the Perzyna model [17] is used. This model relates the dynamic yield stress σ_d by a factor β with the quasi-static yield stress σ_y and the effective plastic strain-rate $\dot{\varepsilon}$ by

$$\sigma_\mathrm{d} = \beta\sigma_\mathrm{y} \quad \text{with} \quad \beta = 1 + \left(\frac{\dot{\varepsilon}}{\gamma}\right)^m . \tag{11}$$

The material viscosity parameter is denoted by γ, and the strain-rate hardening parameter by m. Both parameters have to be obtained from the Split Hopkinson pressure bar test.
In Fig. 3 the quasi-static yield stress for S235 and Al6060 are shown. In Tab. 1 the corresponding material data and Perzyna coefficients are listed. Finite Element simulations of two impacting particles are performed to determine the COR. A schematic representation

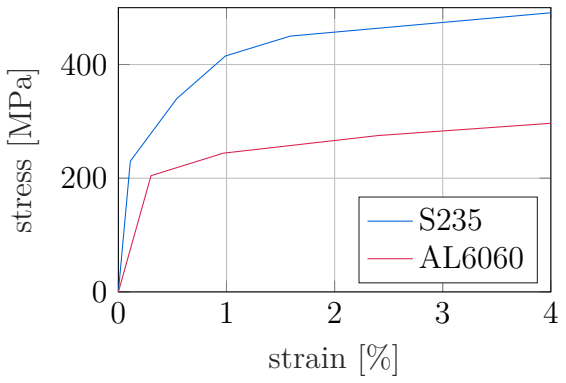

Figure 3: Quasi-static stress-strain curves.

Table 1: Material parameters.

Material	E [GPa]	ν [-]	ρ [kg/m^3]
S235	208	0.3	7800
Al6060	67.7	0.33	2702

σ_y [MPa]	γ [-]	m [-]
230	305	0.403
205	5548	1

of the sphere-sphere model is shown in Fig. 4 (left). The spheres have an initial radius of 5 mm, which can be scaled for different sizes. Each sphere consists of 6093 axis symmetric 2D elements, in ABAQUS called CAX4R. The element size varies between 0.5 mm till 0.015 mm. Both spheres are assigned with half the collision velocity ($\dot{\delta}_\mathrm{a}$) with opposed signs.
The kinematic COR is evaluated by the normal velocities of the spheres before (0) and after (1) the collision of sphere I and II, reading

$$e = \frac{v_\mathrm{I}^1 - v_\mathrm{II}^1}{v_\mathrm{I}^0 - v_\mathrm{II}^0}. \tag{12}$$

The velocities before impact are priori known. The velocities after impact are evaluated at the reference points of the spheres. The mean value of the last 200 time steps is taken, as the velocity is oscillating a little bit due to mechanical vibrations of the spheres, which are induced thru the collision. If instead of a sphere-sphere contact a sphere-wall contact is simulated one sphere is replaced by a wall. The wall is modeled as a cylinder with its diameter and length being the diameter of the sphere. The contour of the cylinder is completely clamped. In the later DEM simulations steel spheres of 5 mm radius will be used. The box is made of aluminum. For these settings, the COR is shown in Fig. 4 (right). A high dependency on the impact velocity is observed. For both settings the COR is close to one for small impact velocities. When the impact velocity increases the COR starts to decrease rapidly. For high velocities the COR drops to 0.5 till 0.4.

5 Experimental and numerical investigations

To check the experimental measurement system the empty particle box is analyzed first. As only minor damping effects, arising from the boundary condition or material damping, exist the energy dissipation is very small. The mean value of the loss factor is about 0.01. In the next step, particles are filled in the box. Unhardened, steel balls made of V2A, which are used in the hardened form for ball bearings, are utilized. These have a high degree of roundness and accurate material parameters are available for the later simulation purposes. For the first setup, 58 of 62 maximum possible particles with a radius of 5 mm are used. The total weight of the particles is 241 g.
The energy dissipation and loss factor for this setting are shown in Fig. 5. From the loss factor a high energy dissipation over a big area of the measurement range can be observed. The mean loss factor is 0.18, which is eighteen times higher than in the empty case. The loss factor is especially high for medium frequencies (60 Hz - 150 Hz) or medium accelerations (20 m/s^2 - 70 m/s^2) with an value up to 0.7. Only at high frequencies (>200 Hz) and high accelerations (>100 m/s^2) the dissipation is comparatively small. The minimum value of the loss factor is here only 0.03. In the area of high frequencies (≈800 Hz) and low accelerations (≈10 m/s^2) the loss factor becomes unrealistic high. However, in this area the energy of the system is very low and inaccuracies in the force signal have a bigger effect on the result. At the lower border of the frequency range (<60 Hz) and acceleration range (<20 m/s^2) the loss factor starts to drop, showing that here another ineffective area of the particle damper starts.

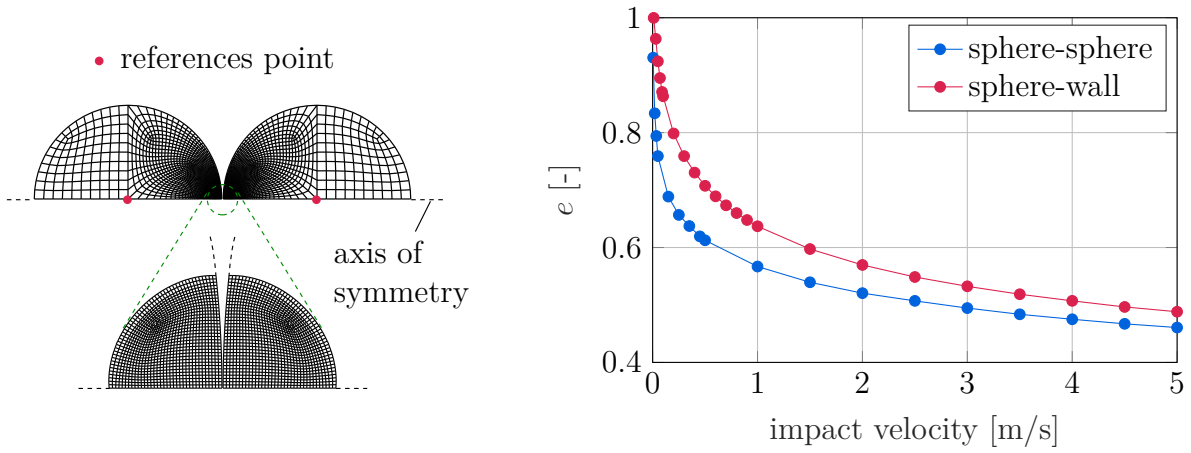

Figure 4: Left: Schematic representation of the FEM model of two impacting spheres.
Right: Velocity dependent COR for a sphere-sphere and sphere-wall contact with a size of 10 mm.

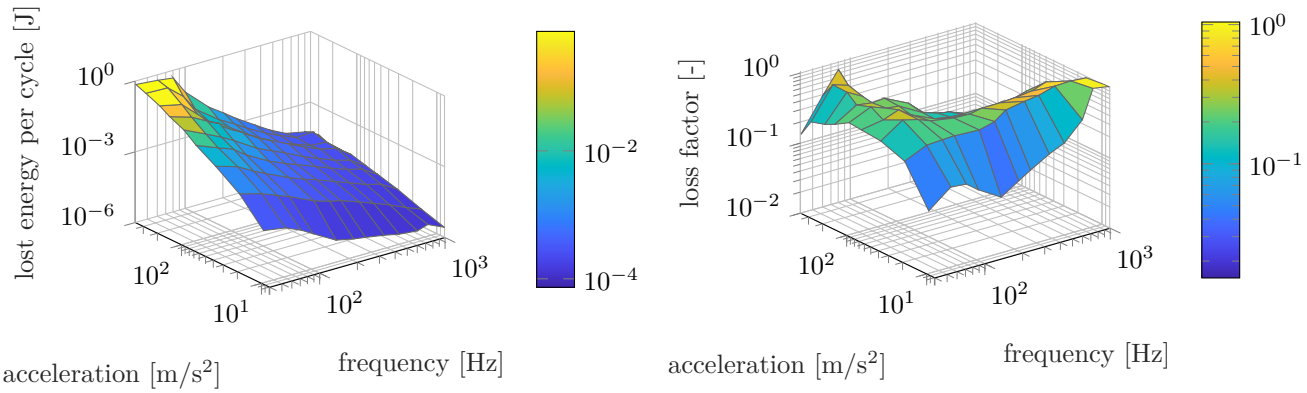

Figure 5: Measured energy dissipation (left) and loss factor (right) with 58 particles of 5 mm radius.

5.1 Numerical investigations of the contact parameters

In the following, the DEM simulation results are compared with the measurements. In order to do so, the measured frequencies and acceleration values are simulated. Each grid point is simulated for 25 periods, whereas the first five periods are cut off to remove the irregular movement of the particles introduced by the initial conditions. The main adjustment parameters are the force laws and their parameters. As normal force the formula of Gonthier (Eq. (7)) is chosen, whereby a constant COR as well as the velocity dependent COR from Fig. 4 are utilized. Indeed, not the exact same materials for the particles are used in the experiment (V2A) as in the FEM simulation (S235), but their characteristics are very similar. For the friction force no friction, sliding friction, see Eq. (10), and sticking friction [12] are analyzed.
The best result between experiment and simulation is achieved with the velocity dependent COR and the sliding friction with $\mu = 0.1$. The relative mean difference of the energy dissipation is 0.36. This setting is thus used for all following simulations. If instead a

constant COR is used, the relative mean difference is 0.44, and the best COR has to be found by excessive tuning. By neglecting friction the minimal relative mean difference becomes 0.43. Taking the sticking friction algorithm the relative mean difference is 0.36, but the simulation time is much higher as with the sliding friction algorithm.

In Fig. 6 the simulation results for the chosen contact parameters are compared to the measured results. The biggest differences occur at low accelerations (<20 m/s^2) and high frequencies (>250 Hz). Indeed, this area is also prone to measurement inaccuracies of the force signal. Also, around 400 m/s^2 and 100 Hz there is a small area where the difference is much bigger as in the surroundings. In this area an offset in the energy dissipation curves is observed and outside this area both curves agree well. This shows that the simulations meet the qualitative characteristics of the energy dissipation very well, with some quantitative differences in its magnitude. However, besides the quantitative discrepancies the simulations are very useful to give qualitative insights on the complex dynamics inside the damper.

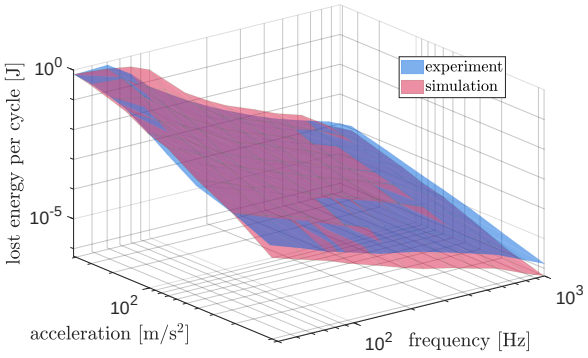

Figure 6: Comparison of experimental and numerical results for the energy dissipation.

One special characteristic of particle dampers is the complex movement of the particles. In the following, it is analyzed by simulation how this movement and the contact parameters are affecting the energy dissipation of the dampers for different periods. For this purpose, the energy dissipation is directly calculated by the given force laws. In Fig. 7 (left) the relative standard deviation of the energy dissipation is given for the four edge points of the measurement range for one and for 20 periods. For only one period the relative standard derivation is comparably high. Especially at high frequencies this is the case. However, combining 20 periods reduces the standard deviation significantly. Thus, in the simulations 20 periods are used for the calculation of the complex power.

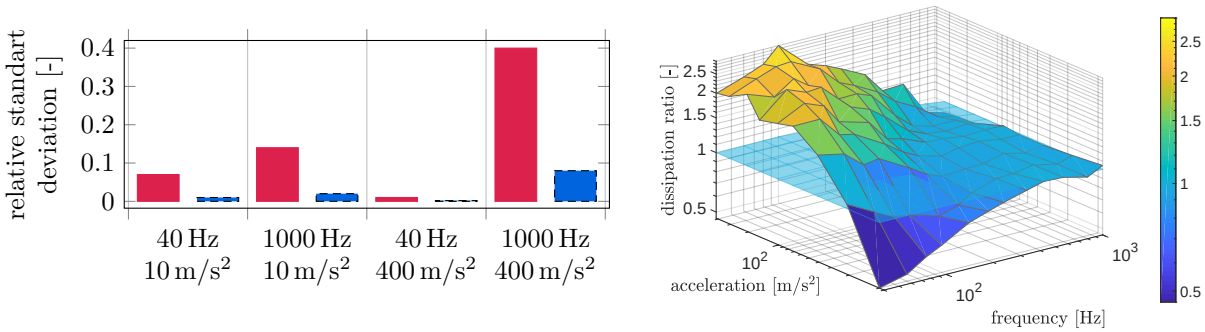

Figure 7: Left: Relative standard deviation of energy dissipation for one (■) and 20 (■) periods. Right: Ratio of dissipated energy of normal contacts to frictional contacts.

In Fig. 7 (right) the ratio of the energy dissipation of normal contacts to frictional contacts is shown. There exist three major regions, i.e. the energy dissipation is dominated by the normal contacts, by friction or is on the same scale. For low frequencies (<100 Hz) and low accelerations (<40 m/s^2) the dissipation is dominated by friction by a factor up to two. When the acceleration is increased, the dissipation becomes dominated by the normal contacts up to a factor of three. For high frequencies (>250 Hz), independent of the acceleration, both dissipation effects are on the same scale. Especially in this area the highest standard deviations for the energy dissipation are determined, as seen in Fig. 7 (left).

5.2 Filling ratio of the particle box

In the next step, different filling ratios of the particle box are analyzed using the experiment and simulation. In addition, to the 58 particles, 40 and 62 particles are utilized, with 62 being the maximum possible particle number. Here as well, a good qualitative agreement between simulation and experiment is obtained. An extended frequency and acceleration range is investigated using the simulation with 20 grid points for the frequency and acceleration values. The frequency varies between 10 Hz till 1 kHz and the acceleration between 10 m/s^2 till 1000 m/s^2. The results for the lost energy are shown in Fig. 8. Comparing, 40 with 58 particles in Fig. 8 (left), one can see that the 58 particles perform better for frequencies above 70 Hz. For frequencies below 70 Hz there is a strong dependency on the acceleration. The 40 particles are here especially suited for the higher accelerations. The energy dissipation in this area is dominated by the normal contacts, which dissipate up to five times more energy as the frictional losses. A similar behavior is seen by comparing 58 with 62 particles in Fig. 8 (right), but with shifted values. For frequencies below 70 Hz, the 58 particles perform always better as the 62 particles. For higher frequencies indeed, a high dependency on the acceleration is observed again. Here, the 62 particles are especially suited for medium to high accelerations (>40 m/s^2), whereby the energy dissipation by the normal and tangential forces in this area is on the same scale. The different dissipation values can be explained by the varying particle activities [18]. The higher the particle activity is, the higher is the energy dissipation.

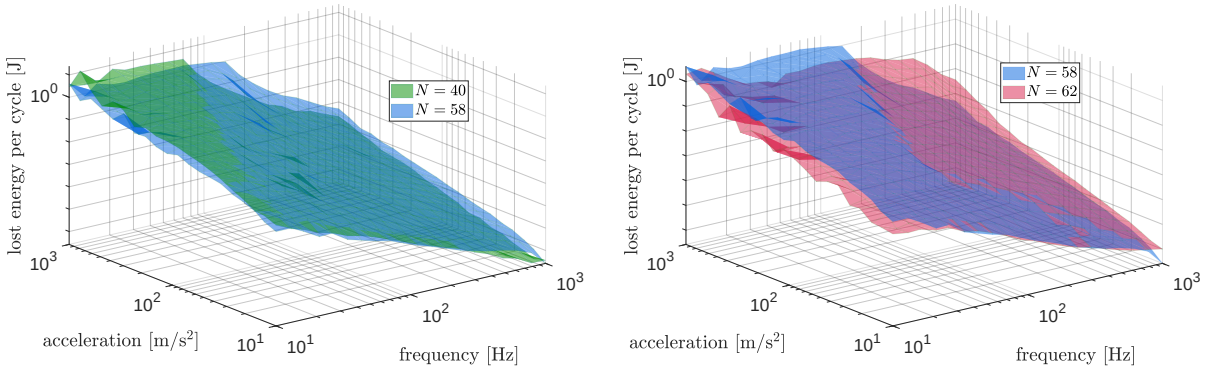

Figure 8: Simulated energy dissipation for 40 vs. 58 particles (left) and 58 vs. 62 particles (right).

Important factors seem to be amongst others the excitation frequency and acceleration, the particle inertia, the available space to move for the particles and their material.

6 Conclusion

An experimental based model and a numerical model for the determination of the energy dissipation and the loss factor of particle dampers alone are presented. Excluding the underlying vibrating structure and concentrating on the particle damper, enables to make general statements about the energy dissipation effects in a single particle damper. Thereby, a large frequency and acceleration range is analyzed. A significant energy dissipation is determined with a high loss factor for specific excitations showing the high potential of particle dampers. A good agreement between experiment and simulation is achieved. The dissipation effect varies between normal contacts and frictional effects, depending on the given excitation. Also, the filling ratio of the particle box showing a big influence on the dissipation energy, as for different frequency areas different filling ratios are better suited. With this parameter, a particle damper can be tuned for a specific excitation, and thus maximizing the damping of the underlying structure. First comparisons of experiments and simulations showing a good qualitative agreement, enabling the simulation as a future design tool for a target-oriented particle damper design. Though, some quantitative differences remain and are focus of future research.

Acknowledgments.

The authors would also like to thank the German Research Foundation (DFG) for their financial support of the project SE1685/5-1.

REFERENCES

[1] H. Panossian, Structural damping enhancement via non-obstructive particle damping technique, Journal of Vibration and Acoustics 105 (114).

[2] N. Meyer, R. Seifried, Numerical and experimental investigations in the damping behavior of particle dampers attached to a vibrating structure, Preprint Reihe des SPP 1897 Calm, Smooth, Smart (7).

[3] N. Meyer, R. Seifried, An experimental model for the analysis of energy dissipation in particle dampers, PAMM 19 (1), accepted.

[4] M. Y. Yang, G. A. Lesieutre, S. Hambric, G. Koopmann, Development of a design curve for particle impact dampers, Noise Control Engineering Journal 53 (2005) 5–13.

[5] P. A. Cundall, O. D. L. Strack, Discrete numerical model for granular assemblies, International Journal of Rock Mechanics and Mining Sciences and Geomechanics 16 (4) (1979) 77.

[6] F. Fleissner, T. Gaugele, P. Eberhard, Applications of the discrete element method in mechanical engineering, Multibody System Dynamics 18 (1) (2007) 81–94.

[7] T. Pöschel, Computational Granular Dynamics: Models and Algorithms, Springer, Berlin, 2005.

[8] H. Hertz, The principles of mechanics : presented in a new form, new dover ed; unabridged and unaltered republication of the 1. ed. Edition, Dover books, Dover Publ, New York, NY, 1956.

[9] H. M. Lankarani, P. E. Nikravesh, A contact force model with hysteresis damping for impact analysis of multibody systems, Journal of Mechanical Design 112 (3) (1990) 369–376.

[10] Y. Gonthier, J. McPhee, C. Lange, J.-C. Piedbœuf, A regularized contact model with asymmetric damping and dwell-time dependent friction, Multibody System Dynamics 11 (3) (2004) 209–233.

[11] S. Andersson, A. Söderberg, S. Björklund, Friction models for sliding dry, boundary and mixed lubricated contacts, Tribology International 40 (4) (2007) 580–587.

[12] A. Di Renzo, F. P. Di Maio, An improved integral non-linear model for the contact of particles in distinct element simulations, Chemical Engineering Science 60 (5) (2005) 1303–1312.

[13] C. W. Gear, The numerical integration of ordinary differential equations of various orders, Mathematics of Computation 21 (98) (1967) 146.

[14] W. Goldsmith, Impact: The Theory and Physical Behavior of Colliding Solids, Edward Arnold Publishers, London, 1960.

[15] T. Pöschel, N. V. Brilliantov, Extremal collision sequences of particles on a line: Optimal transmission of kinetic energy, Physical Review E 63 (2).

[16] R. Seifried, H. Minamoto, P. Eberhard, Viscoplastic effects occurring in impacts of aluminum and steel bodies and their influence on the coefficient of restitution, Journal of Applied Mechanics 77 (4).

[17] P. Perzyna, Fundamental problems in viscoplasticity, in: Advances in Applied Mechanics, Vol. 9, 1966, pp. 243–377.

[18] C. Gnanasambandham, M. Stender, N. Hoffmann, P. Eberhard, Multi-scale dynamics of particle dampers using wavelets: Extracting particle activity metrics from ring down experiments, Journal of Sound and Vibration 454 (2019) 1–13.